

# MOTIONFLOW: LEARNING IMPLICIT MOTION FLOW FOR COMPLEX CAMERA TRAJECTORY CONTROL IN VIDEO GENERATION

**Anonymous authors**

Paper under double-blind review

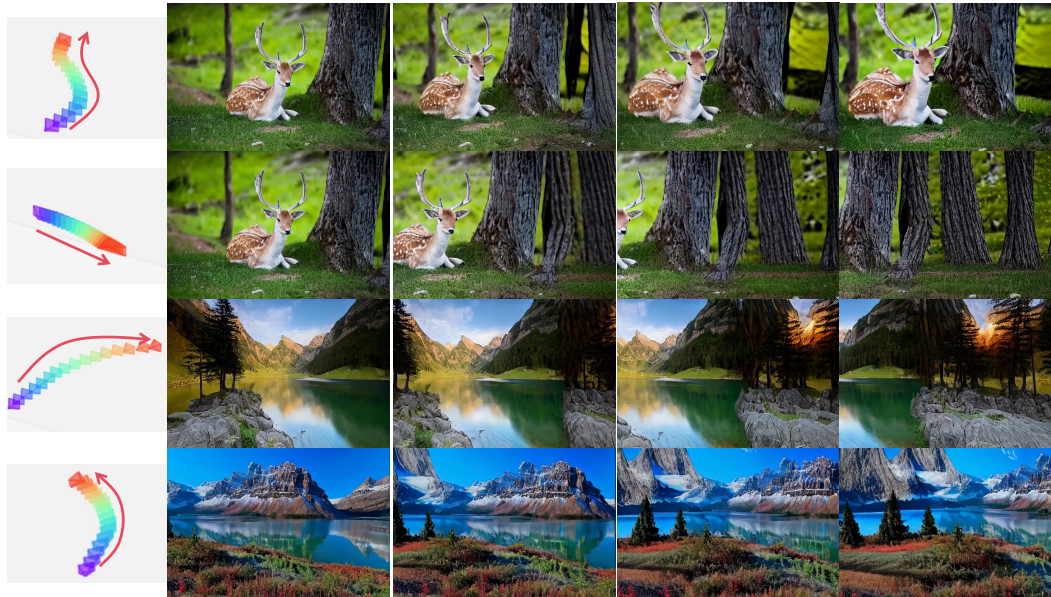


Figure 1: Our method faithfully generates highly realistic and multi-view consistent videos from the given camera trajectory and reference image.

## ABSTRACT

Generating videos guided by camera trajectories poses significant challenges in achieving consistency and generalizability, particularly when both camera and object motions are present. Existing approaches often attempt to learn these motions separately, which may lead to confusion regarding the relative motion between the camera and the objects. To address this challenge, we propose a novel approach that integrates both camera and object motions by converting them into the motion of corresponding pixels. Utilizing a stable diffusion network, we effectively learn reference motion maps in relation to the specified camera trajectory. These maps, along with an extracted semantic object prior, are then fed into an image-to-video network to generate the desired video that can accurately follow the designated camera trajectory while maintaining consistent object motions. Extensive experiments verify that our model outperforms SOTA methods by a large margin. Please visit our anonymous project page to watch the generated videos.

## 1 INTRODUCTION

Through extensive and in-depth research on diffusion models (Song et al., 2020; Saharia et al., 2022; Yu et al., 2023), researchers have significantly improved the quality and diversity of video generation. Recent models, such as DynamicCrafter (Xing et al., 2023), exhibit the ability to generate long,

054 high-quality videos with complex dynamics. However, these methods focus on prompts like texts,  
055 images, depth maps, contour maps, human pose or projection maps (Guo et al., 2023a; Hu et al., 2023;  
056 Guo et al., 2023b; Li et al., 2023; Mou et al., 2023; Peruzzo et al., 2024; Wu et al., 2023; Zhang &  
057 Agrawala, 2023; Hu et al., 2023), often neglecting the precise control over camera motions, which is  
058 essential in applications such as film production, virtual reality (VR), and augmented reality (AR).  
059 These fields require not only high-quality video contents but also precise adherence to specified  
060 camera movements to achieve the desired visual effects.

061 To enable precise camera control in video generation, several strategies have been developed to  
062 integrate trajectory information into generative networks. Although they have made certain progress  
063 in improving the flexibility in control and video quality, the generalizability and consistency still need  
064 improvement. AnimateDiff (Guo et al., 2023b) aggregate camera information through LoRA (J. et al.,  
065 2022) to conditionally guide video generation along specific directions. However, its flexibility is  
066 limited when handling user-customized camera trajectories. MotionCtrl (Wang et al., 2024c) utilizes  
067 the camera transformation matrix as trajectory information and injects it into the generative model. It  
068 employs separate modules to learn camera and object motions, allowing independent motion control  
069 in small-scale scenes such as indoor scenes. Nevertheless, Training the two types of motion separately  
070 while ignoring their relationship may lead to confusion regarding the relative positions of objects and  
071 the scene. Additionally, its relatively simple encoding of camera information restricts its applicability  
072 to precise camera control for large-scale outdoor scenes. CameraCtrl (He et al., 2024) adopts plucking  
073 embeddings (Sitzmann et al., 2021) as the primary camera trajectory representation, which enhances  
074 the implicit mapping between camera motion and pixels. However, the generalizability is still limited,  
075 as it struggles to generate videos that differ substantially from the training data. Additionally, these  
076 methods primarily support text prompt inputs, which often fail to accurately convey the visual details  
of the desired video.

077 To address the above issues, we propose MotionFlow, a novel video generation network guided by  
078 camera trajectories, which is capable of producing consistent and coherent 3D videos. Considering the  
079 limited visual information provided by text guidance, we instead opt for image guidance to accurately  
080 capture the desired video details. Unlike previous methods that modeled camera trajectories and  
081 object motions separately to guide the video generation process, we adopt a pre-trained image stable  
082 diffusion model that progressively and synchronously interacts with both camera motions and image  
083 semantic features. This approach enables us to jointly encode semantic information as object-aware  
084 motion priors during video generation. By mapping camera and object motions onto pixel trajectories  
085 and training a network to learn these pixel movements, we effectively avoid the confusion associated  
086 with separate learning methods.

087 Our network is built on AnimateDiff (Guo et al., 2023b), a pre-trained image-to-video generation  
088 framework, to leverage its high-quality video generation capabilities. To enable precise camera  
089 trajectory-guided control and ensure the generalizability of the method across various scenarios, we  
090 employ an image stable diffusion network to progressively fuse the features of the reference image  
091 with the camera motion trajectory. This information is iteratively injected into the video generation  
092 network using cross attention mechanism as a pixel motion prior. Moreover, to directly enhance the  
093 geometric consistency of the synthesized videos, we implicitly learn the semantic object features from  
094 the reference image and incorporate them into the video generation network through cross-attention  
095 mechanism using these features. This approach improves the quality of the synthesized video frames  
096 that contain the semantic objects during the iterative denoising steps of the diffusion model. Extensive  
097 experimental results demonstrate that our method demonstrates superior 3D consistency, visual  
quality, and camera trajectory controllability compared to previous approaches.

098 We summarize our main contributions as follows:  
099

- 100 • We introduce a framework that iteratively uses an image diffusion network to learn implicit  
101 pixel-level motion flows from camera trajectories and image guidance jointly, achieving  
102 high-quality video generation results that adhere to the input camera trajectories.
- 103 • We propose to extract semantic object information from the image guidance to enable the  
104 video generation network to be aware of these objects through object attention, thereby  
105 improving the quality of these objects' pictures in the generated videos.
- 106 • We conduct extensive experiments to demonstrate the superiority of our MotionFlow network  
107 over SOTA methods both qualitatively and quantitatively.

## 2 RELATED WORKS

### 2.1 CONDITIONAL IMAGE TO VIDEO GENERATION

Conditional image to video (I2V) generation aims to synthesize videos guided by user-provided cues. Recent methods often leverage diffusion models for their stability in training and flexibility in manipulation. Ni et al. (2023) proposes to generate latent flow sequences using a non-pretrained diffusion model to animate images. Their work effectively synthesizes motions like facial expression, human actions, and gestures against an almost static background. Shi et al. (2024) introduce a two-stage training approach, each utilizing a diffusion model to generate explicit motion maps and corresponding video. Although these methods could produce vivid motions in open-domain scenarios, they can not incorporate explicit and precise camera control for the video generation task.

### 2.2 VIDEO GENERATION WITH CAMERA CONTROL

To facilitate camera control, most methods typically use text prompts and specific camera movement information to guide the generation of corresponding videos through cross-modal large models.

To effectively control camera motion, AnimateDiff (Guo et al., 2023b) employs the motion LoRA modules to enable specific camera movements, though quantitative control can be challenging. Focusing on the explicit control of both camera and object motion, MotionCtrl (Wang et al., 2024c) achieves flexible motion control. However, its camera motion control module relies on 12 pose matrix parameters as input, which may not sufficiently capture the geometric cues needed for precise camera control. Direct-a-video (Yang et al., 2024) proposes a camera embedder to manipulate camera poses, but it only conditions on some basic camera parameters (such as pan or zoom), limiting its control capabilities. In contrast, CameraCtrl (He et al., 2024) adopts plücker embeddings as the camera trajectory parameters, effectively injecting the camera information. Based on this embedding, VD3D (Bahmani et al., 2024) and CamCo Xu et al. (2024) respectively introduce a ControlNet-like conditioning mechanism and an epipolar attention module to better incorporate camera embeddings. Our method further employs a twin diffusion model to encode these plücker embeddings, allowing for the adaptive and progressive introduction of camera pose information during the iterative denoising process of the diffusion model. Additionally, we enhance plücker embeddings into progressive implicit embeddings, further improving global consistency and stability in the generated videos.

By adopting image prompts, our approach provides a more direct and accurate condition for generation. Moreover, it can be combined with cross-modal large models to facilitate multi-stage, text-driven video generation.

## 3 METHOD

The core idea of our method involves the progressive injection of semantic and pixel-level motion information into a diffusion-based video generation network. As illustrated in Figure 2, we employ a reference motion network to extract pixel-level motion with semantic information from a reference image and a camera trajectory, which serves as a motion flow to guide video generation through reference attention. To further identify potential moving foreground objects and stationary backgrounds within the scene, we introduce a semantic extractor to capture semantic information. This information is then injected into the video generation network through both pixel-wise addition and object attention. For the video generation network, we utilize the pre-trained model of AnimateDiff (Guo et al., 2023b), enhancing it by incorporating reference attention and object attention in each block of the UNet architecture.

This section is structured as follows: Section 3.1 provides a brief overview of the base video generation network; Section 3.2 delves into the camera encoding information; Section 3.3 discusses the integration of semantic information into the video generation backbone network; Section 3.4 explores the incorporation of pixel motion, generated by the reference motion network, into the video generation framework to progressively guide the process; Finally, Section 3.5 presents a detailed analysis of pixel-level motion with semantic and camera motion information.

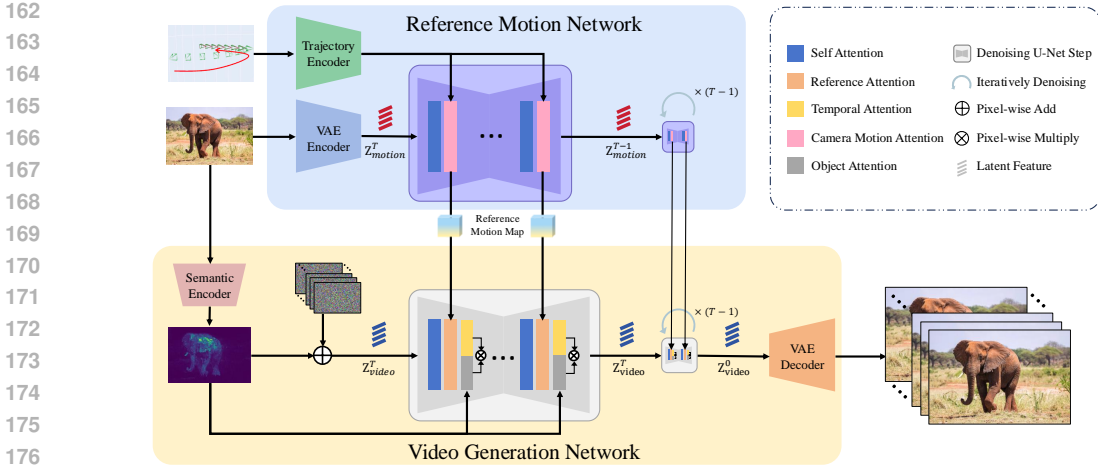


Figure 2: The overview of *MotionFlow*. Our framework is mainly constituted of two parts. In the reference motion network, the camera trajectory is initially encoded using Trajectory Encoder and added to the reference model using camera motion attention with the reference image to get the reference motion priors. For the video diffusion process stage, firstly semantic features are extracted through the semantic encoder to calculate the object attention and also fused with multi-frame noise. Secondly, reference pixel motion is integrated through reference attention. In addition, Temporal Modules are utilized to ensure consistency of generated video.

### 3.1 VIDEO DIFFUSION MODELS

Video diffusion models are a class of generative models that extend the principles of diffusion probabilistic models for image generation to the domain of video synthesis. These models learn to reverse a gradual noising process applied to video sequence data, enabling the generation of high-quality, temporally coherent video sequences. Let  $x_0 \in \mathbb{R}^{f \times h \times w \times c}$  represent a video latent with  $f$  frames, each with dimensions  $h \times w$  with  $c$  channels. The forward diffusion process is defined as a Markov chain that gradually adds Gaussian noise to the original video:

$$x_t = \sqrt{\bar{a}_t}x_{t-1} + \sqrt{(1 - \bar{a}_t)}\varepsilon, \varepsilon \sim N(0, 1), \quad (1)$$

where  $t \in 1, \dots, T$  denotes the diffusion step,  $\bar{a}_t$  is a noise scheduler and  $\varepsilon$  is sampled from a standard Gaussian noise. The model learns to reverse this process, estimating  $p(x_{t-1}|x_t)$ , typically parameterized by a neural network  $\theta$ . The objective is to minimize the loss:

$$\mathcal{L}(\theta) = \mathbb{E}_{x_0, \varepsilon, cond, t} [\|\varepsilon - \hat{\varepsilon}_\theta(x_t, cond, t)\|_2^2], \quad (2)$$

where *cond* represents the conditioning inputs, which may include textual prompts, reference images, camera trajectories, and scene outlines. Video diffusion models incorporate spatiotemporal architectures to capture both spatial details and temporal dynamics. They generally employ mechanisms such as 3D convolutions, attention layers, or recurrent structures to ensure consistency across frames. These models have demonstrated remarkable capabilities in tasks such as video generation, editing, and motion transfer, pushing the boundaries of video synthesis quality and controllability.

### 3.2 TRAJECTORY ENCODER

The trajectory of camera motion can be represented through the transformation of the camera between various frames within a video sequence. This transformation can be succinctly described using the rotation matrix  $\mathbf{R} \in SO(3)$ , and the translation matrix  $\mathbf{t} \in \mathbb{R}^3$ . MotionCtrl (Wang et al., 2024c) represents camera motion by flattening camera parameters into 12D vectors and concatenating them with time embeddings from the base video generation network. A lightweight fully connected network then ensures dimensional consistency between the new combined embeddings and the original time embeddings. However, this representation has limitations in accurately describing camera motion for two primary reasons: 1. Camera parameters inherently reflect characteristics of the camera space,

where rotation matrices and translation vectors carry distinct semantic meanings and should be treated separately rather than flattened into a single vector. 2. Modeling the correlation between raw camera parameters and pixel space is challenging, potentially limiting the model’s generalization capacity, particularly for large-scale complex outdoor scenes. In order to better describe the camera pose, we use plücker embeddings (Sitzmann et al., 2021) as the representation of camera trajectory. Given the extrinsic and intrinsic camera parameters  $\mathbf{R}, \mathbf{t}, \mathbf{K}_f$  for the  $f$ -th frame, we derive a plücker embedding  $\ddot{\mathbf{p}}_{f,h,w} \in \mathbb{R}^6$  for each pixel located at  $(h, w)$ . This embedding represents the vector from the camera center to the pixel’s position as:

$$\ddot{\mathbf{p}}_{f,h,w} = \left( \mathbf{t}_f \times \hat{\mathbf{d}}_{f,h,w}, \hat{\mathbf{d}}_{f,h,w} \right), \quad \hat{\mathbf{d}}_{f,h,w} = \frac{\mathbf{d}}{\|\mathbf{d}_{f,h,w}\|}, \quad \mathbf{d}_{f,h,w} = \mathbf{R}_f \mathbf{K}_f [w, h, 1]^\top + \mathbf{t}_f \quad (3)$$

Computing plücker embedding for each pixel results in a representation  $\ddot{\mathbf{P}} \in \mathbb{R}^{6 \times F \times H \times W}$  for a specified trajectory. To inject the trajectory representation into the reference motion network, we designed a trajectory encoder structurally similar to the camera encoder in CameraCtrl (He et al., 2024). However, we improved the architecture: after each 2D ResNet block, we replaced the temporal attention with self-attention and output multi-scale trajectory features.

### 3.3 SEMANTIC ENCODER

We design a semantic encoder to extract the semantic features of salient objects to let the video generation network be aware of these objects. To achieve this, one feasible way is to mark the area of these objects and send it to object attention modules, as shown in the Figure 2. To get these fine-grained information, our semantic encoder employs a lightweight ViT architecture (Caron et al., 2021) to adaptively identify potential areas of salient objects. This module is trained in the first stage, which will be explained in detail in Section 3.6.

### 3.4 REFERENCE MOTION NETWORK

Recent works mainly rely on textual prompts combined with camera features for the camera trajectory control in video generation (He et al., 2024; Wang et al., 2024c). However, due to the loss of scene details in the prompts, it is difficult for them to accurately learn the features to represent the motion of foreground objects and background scenes, potentially leading to low-quality results. Therefore, images are often preferred in I2V tasks since they can convey more fine-grained scene details compared to textual prompts. Some methods (Chen et al., 2023; Xing et al., 2023) adopt CLIP image features in place of CLIP text features and feed them into the diffusion network through cross-attention to achieve image guidance. However, the CLIP features emphasize the text-image alignment and are learned with low-resolution(224×224) image input, which still prioritize high-level abstraction of images and ignore image details.

Another approach is to leverage the ControlNet architecture (Zhang et al., 2023) to achieve camera trajectory control. While this approach can utilize different conditional information to guide video generation, its key limitation is that the supplementary conditional information must be well-aligned with the underlying image features to enable effective interaction. Yet, the trajectory information in camera space and the features in image space exist in different domains, making it challenging for ControlNet to directly convert the trajectory information into motion guidance that the video generation network can understand. Furthermore, the lack of high-quality video data that contains precise camera poses also hinders the generalization capability of such approaches, as discussed in Section 4.2,.

Our idea is to introduce a separate reference motion network to integrate the camera motion trajectory and the semantic information of the reference image, directly producing reference motion maps that can be used in the image space. Specially, as shown in Figure 2, this network adopts a pretrained image stable diffusion(SD1.5 Unet<sup>1</sup>) architecture (Voleti et al., 2024) that incorporates both self and cross-attention layers within the spacial transformer. We inject the multi-scale camera features into

<sup>1</sup><https://huggingface.co/stable-diffusion-v1-5/stable-diffusion-v1-5>

the cross-attention layers to effectively capture semantic pixel motions as

$$F_{\text{out}} = \text{Softmax}\left(\frac{QK_i^T}{\sqrt{d}}\right) V_i + \lambda_c \cdot \text{Softmax}\left(\frac{QK_c^T}{\sqrt{d}}\right) V_c, \quad (4)$$

where  $Q = \varphi_i(z_t) W_z$ , with  $\varphi_i(z_t) \in \mathbb{R}^{N \times d_i}$  representing the spatially flattened tokens of the video latent. Here,  $K_i = \Psi(\text{img})W_{ki}$  and  $V_i = \Psi(\text{img})W_{vi}$ , where  $\Psi$  denotes the CLIP image encoder. Similarly,  $K_c = \Phi(\text{cam})W_{kc}$  and  $V_c = \Phi(\text{cam})W_{vc}$ , with  $\Phi$  representing the Trajectory Encoder. The parameter matrices is denoted by  $\mathbf{W}$ , and  $\lambda_c$  is the coefficient that balances image condition and camera condition.

The weighted combination of camera and image conditions in the cross-attention allows the reference motion network to integrate the encoded camera trajectory with the initial image features effectively. Through end-to-end training, the network is able to predict reference motion maps that contain pixel-level motion information caused by camera pose changes in a frame-by-frame manner. These maps are then injected into the base video generation network through reference attention, as detailed in section 3.5

### 3.5 VIDEO GENERATION NETWORK

We adopt AnimateDiff (Guo et al., 2023b) as the foundation of our video generation network. We utilize the camera-related frame-by-frame reference motion maps generated by the reference motion network to guide pixel-level motion in the video generation process. Specifically, for each block of the video generation network, given the feature map  $m_i \in \mathbb{R}^{f \times c \times h \times w}$  from the  $i$ -block of the base network and the pixel motion  $p_i \in \mathbb{R}^{f \times c \times h \times w}$  from reference motion network, we concatenate  $p_i$  with  $m_i$  along the  $w$  dimension to obtain  $m'_i \in \mathbb{R}^{f \times c \times h \times 2w}$ . Then we perform cross-attention and extract the first half along the  $w$  dimension of the  $m'_i$  as the input of the objection attention, referred to as reference attention. As described in Section 3.3, we subsequently employ the semantic encoder to capture semantic information, addressing potential moving foreground objects and stationary backgrounds. This information is injected into the video generation network through addition and object attention operations, as illustrated in Figure 2. We not only integrate semantic information during the noise input process but also compute an attention map as a semantic mask between the semantic feature map and the output of reference attention, referred to as object attention. Simultaneously, inspired by the architectural concepts of AnimateDiff (Guo et al., 2023b), we apply temporal attention to the output of reference attention to consolidate consistency between consecutive frames. Specifically, we reshape the input feature map  $m_i \in \mathbb{R}^{c \times f \times h \times w}$  to the shape  $(h \times w) \times f \times c$ . Then we calculate the self-attention across the temporal dimension  $f$ . The final result is then pointwise multiplied with the semantic mask to produce the output of this block.

### 3.6 TRAINING STRATEGY

The video generation network is initialized using the pre-trained weights from AnimateDiff (Guo et al., 2023b), while the reference motion network is initialized with the pre-trained Stable Diffusion V1.5 (Rombach et al., 2022) model. The semantic encoder is initialized from ViT-S based DINO (Caron et al., 2021). All other modules are initialized to zero. The MotionFlow is trained using the Adam optimizer (Kingma & Ba, 2015),  $8 \times$  GPUs, and batch size of 1 per GPU. In the first stage, we train the Trajectory Encoder and motion extractor with a learning rate of  $1e^{-4}$  for one day, keeping the reference motion network and video generation network fixed. Subsequently, we train all parts for three days with a reduced learning rate of  $1e^{-5}$ . We use RealEstate10K dataset (Zhou et al., 2018) for training, which consists of 62 992 video clips for training and 7 391 video clips for testing accompanied by diverse camera trajectories. To further evaluate the generalizability of our model, we test it on the large-scale outdoor dataset DL3DV-10k (Ling et al., 2024), which contains approximately 10 000 videos with known camera poses as well as the generation of videos for animals.

## 4 EXPERIMENTS

Our experiments are conducted on a server equipped with  $8 \times$  NVIDIA A800 GPUs. To better evaluate the control of camera trajectories, we designed separate comparisons for small-scale and

large-scale camera movements. Specifically, we conducted experiments to compare the geometric consistency of the generated videos, the semantic consistency, and the alignment between the camera trajectories and the target videos. Experimental results also reveal that our method can generate high-quality videos for dynamic scenes that contain the motion of a part of active foreground objects, such as the head movement of an animal.

CameraCtrl (He et al., 2024) and MotionCtrl (Wang et al., 2024c) are three baseline methods that are most relevant to our method. To ensure fair comparisons, we trained all the methods on the RealEstate10K (Zhou et al., 2018) dataset and tested them using the same camera trajectories and image prompts. To validate the generalizability of our model, we compare our model with other image-to-video generation models on DL3DV-10k(Ling et al., 2024), which is new to all the models.



Figure 3: Qualitative Results. Given a reference image (the topmost image of each group), our approach demonstrates the ability to any camera trajectory. The illustration showcases results with clear, consistent details, and continuous motion.

#### 4.1 METRICS

We evaluate our method from two aspects: the alignment of camera trajectories and the visual quality of the generated videos. The distance between predicted and ground-truth camera trajectories is used to measure the alignment. Specifically, we predicted the camera trajectories for both the generated and real videos using the same methods to eliminate the potential scale differences caused by different Structure-from-Motion techniques. Considering the scale and differences between the rotation and translation parameters in the camera matrix, we use *rotation error* and *translation error* to assess them individually, following the approach of Wang et al. (2024c); He et al. (2024).

Four classical image-level quality metrics, including Fréchet Inception Distance (FID) (Heusel et al., 2017), SSIM (Wang et al., 2004), PSNR (Hore & Ziou, 2010) and LPIPS (Zhang et al., 2018), are used to evaluate the quality of the generated video frames, and video-level metric Fréchet Video Distance (FVD) (Unterthiner et al., 2018) is further applied to assess video-level quality, similar to previous video generation methods(Wu et al., 2023; Khachatryan et al., 2023; Cai et al., 2023b; Ceylan et al., 2023; Cai et al., 2023a).

#### 4.2 COMPARISON WITH STATE-OF-THE-ART METHODS

**Geometric consistency.** The effectiveness of camera-guided control is evaluated with the camera trajectories estimated with the Structure-from-Motion technique. Due to the low overlap between images of RealEstate10K scenes, the commonly used COLMAP (Schönberger & Frahm, 2016) frequently fails to estimate their corresponding camera trajectories. Instead, we used ParticleSfM (Zhao et al., 2022) similar to MotionCtrl(Wang et al., 2024c), a pre-trained network framework capable of estimating camera trajectories in complex and dynamic scenes, to get the camera trajectories of generated videos. We evaluate the rotation part  $R \in \mathbb{R}^{3 \times 3}$ , and the translation part  $T \in \mathbb{R}^{3 \times 1}$  separately.

To fully compare our model and other camera trajectory guided video generation models, we conduct basic trajectory (sample every 8 frames) and difficult trajectory (sample every max frame we can sample). To guarantee the reliability of the experiment, we evaluated the error between the generated video’s camera trajectory and the ground truth (GT) video trajectory using ParticleSfM (Zhao et al., 2022), Dust3R (Wang et al., 2024b) and VggSfM (Wang et al., 2024a). As shown in Table 1, our method can generate videos that align better with the GT camera trajectories compared to other methods, both in basic and difficult trajectories.

Table 1: Quantitative comparisons (Pose got by Dust3r, VggSfM, and ParticleSfM). We compare against prior work on basic trajectory and random trajectory respectively. T-Err and R-Err, representing TransErr and RotErr respectively, are reported as the metrics from Appendix A.

	Basic Trajectory						Difficult Trajectory					
	Dust3R		VggSfM		ParticleSfM		Dust3R		VggSfM		ParticleSfM	
	T-Err↓	R-Err↓	T-Err↓	R-Err↓	T-Err↓	R-Err↓	T-Err↓	R-Err↓	T-Err↓	R-Err↓	T-Err↓	R-Err↓
CameraCtrl	0.092	0.300	1.499	<b>0.204</b>	2.80	0.924	0.080	0.291	1.711	<b>0.195</b>	3.17	<b>0.648</b>
MotionCtrl	<b>0.059</b>	<b>0.228</b>	<b>0.882</b>	0.215	<b>2.02</b>	<b>0.914</b>	<b>0.054</b>	<b>0.227</b>	<b>1.012</b>	0.226	<b>2.10</b>	<b>0.739</b>
Ours	<b>0.043</b>	<b>0.223</b>	<b>0.767</b>	<b>0.156</b>	<b>1.66</b>	<b>0.886</b>	<b>0.053</b>	<b>0.210</b>	<b>0.802</b>	<b>0.146</b>	<b>1.77</b>	<b>0.574</b>

**Visual Quality.** The image-level and video-level quality metrics are adopted for the video consistency and image quality evaluation. To ensure fair evaluation, all models for comparison are trained on the same dataset RealEstate10K with the same baseline SD1.5. As the the experimental results demonstrated in Table 2 and Figure 4, our model not only generates high-quality videos guided by camera trajectories but also outperforms other methods of the same type in terms of video generation quality, highlighting the effectiveness of our approach. In Figure 1 and Figure 3, we further demonstrate the results of videos generated by our method in indoor, outdoor, and dynamic scenes, showcasing its adaptability and robustness across various video generation tasks.

Table 2: Quantitative comparison on visual quality.

	Basic Trajectory					Difficult Trajectory				
	LPIPS↓	PSNR↑	SSIM↑	FID↓	FVD↓	LPIPS↓	PSNR↑	SSIM↑	FID↓	FVD↓
CameraCtrl	0.791	8.62	0.212	99.83	1079	0.796	7.57	0.17	112.77	1023
MotionCtrl	<b>0.732</b>	<b>9.48</b>	<b>0.266</b>	<b>81.28</b>	<b>972</b>	<b>0.728</b>	<b>8.70</b>	<b>0.24</b>	<b>84.68</b>	<b>789</b>
Ours	<b>0.206</b>	<b>17.5</b>	<b>0.567</b>	<b>38.48</b>	<b>348</b>	<b>0.255</b>	<b>17.7</b>	<b>0.54</b>	<b>41.93</b>	<b>390</b>

**Generalizability Comparison.** The outdoor dataset DL3Dv datasets (Ling et al., 2024) is employed to evaluate the generalizability of models which are trained solely on indoor datasets. As shown in Table 3, our method demonstrates superior image-level and video-level quality with SOTA methods (Xing et al., 2023; Chen et al., 2023; Guo et al., 2023b). This highlights the enhanced robustness and generalizability of our method, which is attributed to the additional diffusion model that progressively facilitates the synchronization of camera pose with the reference image. As a result, it not only improves the original video’s generation capability but also provides better guidance and control. The specific results are shown in Figure 5 and Table 3.

Table 3: Generalization ability of outdoor scenes. IC: image condition.

	Real10k					DL3DV				
	LPIPS↓	PSNR↑	SSIM↑	FID↓	FVD↓	LPIPS↓	PSNR↑	SSIM↑	FID↓	FVD↓
AnimateDiff	0.326	15.22	0.478	55.43	<b>508</b>	0.632	11.04	0.239	<b>64.87</b>	793
VideoCrafter	0.573	11.81	0.338	60.49	708	0.529	12.45	0.280	83.35	901
DynamicCrafter	<b>0.272</b>	<b>16.38</b>	<b>0.523</b>	<b>47.91</b>	589	<b>0.336</b>	<b>14.92</b>	<b>0.339</b>	70.12	<b>719</b>
MotionCtrl	0.763	9.14	0.218	74.84	977	0.776	9.77	0.174	97.54	1116
CameraCtrl+IC	0.479	13.62	0.423	60.89	704	0.554	12.87	0.282	85.21	1006
Ours	<b>0.188</b>	<b>18.70</b>	<b>0.599</b>	<b>22.55</b>	<b>311</b>	<b>0.282</b>	<b>15.64</b>	<b>0.368</b>	<b>55.62</b>	<b>505</b>

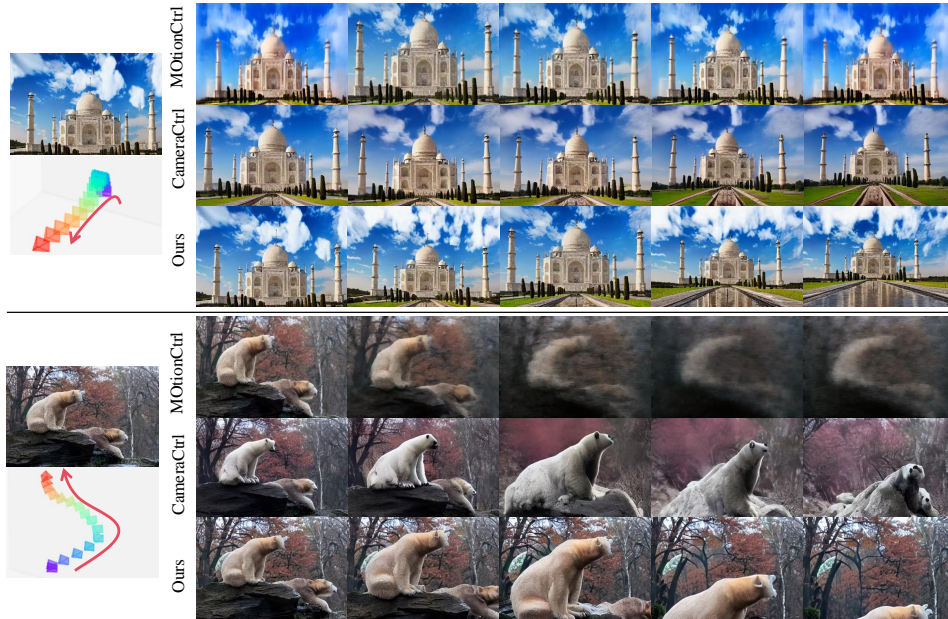


Figure 4: Qualitative comparison on the control ability of and video quality.



Figure 5: Qualitative comparison on the generalization ability of outdoor scenes. Cross-frame misalignment and artifacts are highlighted with red dashed boxes.

### 4.3 ABLATION STUDY AND ANALYSIS

**Reference Motion Network.** We first verified the effectiveness of the reference motion network, the most important module in our model. The first line of the Table 4 shows results generated with the network trained without this network, where the output of trajectory encoder is directly fed into the reference attention of video generation network. Significant drops of all metrics can be observed when training without reference motion maps to provide reference motion flow. We further explored the benefit of using stable diffusion pre-trained parameters for the reference motion network. The results shows that adopting pre-trained parameters leads to an overall improvement, especially the generative quality. This improvement can be attributed to the pre-trained model’s strong 3D priors and image generation capabilities.

**Semantic Extractor.** As the second line of Table 4, the semantic extractor results in an overall improvement. This is because the semantic extractor provides a semantic prior of the reference image to the video generation network, which contributes to the decoupling of various objects with complex motion.

Table 4: Ablation study.

	Visual Quality					Camera Trajectory Alignment	
	LPIPS↓	PSNR↑	SSIM↑	FID↓	FVD↓	TransErr↓	RotErr↓
w/o referNet	0.281	16.58	0.521	41.93	463	1.12	0.297
w/o Semantic Encoder	0.194	18.23	0.561	25.69	319	0.697	0.296
w/o stable diffusion pretrain	0.218	16.87	0.532	39.53	393	0.722	0.299
Full Model	0.188	18.70	0.599	22.55	311	0.608	0.295

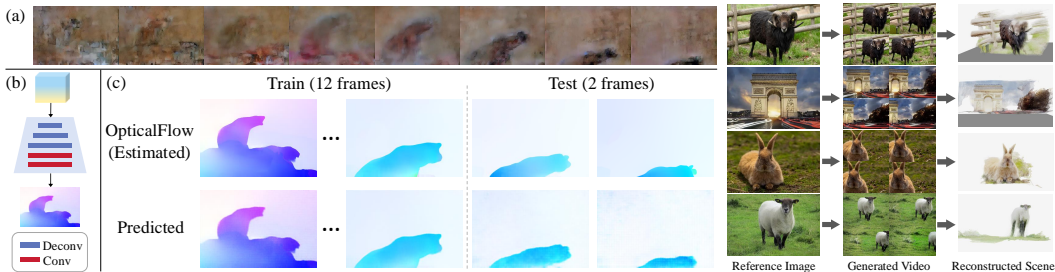


Figure 6: Toy experiment for the Reference Motion Maps interpretation. Figure 7: Scene Reconstruction with generated video.

**Analysis of Reference Motion Maps.** After translating reference motion maps (RMMs) into images through the decoder of the pre-trained VAE, we observe that these images seem to record the salient object movements in generated videos, as shown in the Figure 6 (a). We thus hypothesize that RMMs contain optical flow (OF) information, and conduct a toy experiment to verify it. First, we estimated OFs from a generated video (de Armas, 2019), and then treated them and the corresponding RMMs as data pairs. Here we choose the video shown in the second example of Figure 5 as an example, where the first 12 pairs of RMMs and OFs are taken as the training set and the 2 pairs at the last two frames as the test set. Second, a shallow network is adopted to translate the RMMs to OFs. The network consists of 3 deconvolution (Noh et al., 2015) layers for decoding features to image resolution and 2 convolution layers for feature translation, as shown in Figure 6 (b). We trained the network for 1k epochs with a batch size of 12, L1 loss, and the Adam optimizer, taking approximately 40 seconds. As the results illustrated in Figure 6 (c), the OF information can be directly extracted from RMMs of test frames. While this experiment verifies the correlation between RMMs and OFs, we argue that the learned RMMs have more abundant information than OFs to facilitate the camera trajectory control.

#### 4.4 APPLICATION: 3D SCENE GENERATION

Our method not only retains the original video generation capability of the model but also incorporates camera control. With only a single reference image and a panoramic camera trajectory, we can generate a corresponding scene video and can further perform 3D reconstruction on this video to obtain explicit 3D scenes, as shown in Figure 7.

### 5 CONCLUSION, LIMITATION, AND FUTURE WORK

Through a comparative study with existing camera-guided video generation frameworks, such as CameraCtrl and MotionCtrl, our method demonstrates superior performance in controlling camera movements across different scales. Furthermore, our model also demonstrates a significant advantage in image and video quality compared to other video generation approaches.

Although our method can generate high-quality dynamic scenes while considering potential object motion during camera movement, it lacks explicit guidance for object motion control. In the future, we plan to employ image or point-based motion guidance to precisely control the spatial object movement and the changes over time, while maintaining the generation quality and camera trajectory alignment.

## REFERENCES

- 540  
541  
542 Sherwin Bahmani, Ivan Skorokhodov, Aliaksandr Siarohin, Willi Menapace, Guocheng Qian, Michael  
543 Vasilkovsky, Hsin-Ying Lee, Chaoyang Wang, Jiayu Zou, Andrea Tagliasacchi, DavidB Lindell,  
544 and Sergey Tulyakov. Vd3d: Taming large video diffusion transformers for 3d camera control.  
545 *arXiv:2407.12781*, 2024.
- 546 Shengqu Cai, Duygu Ceylan, Matheus Gadelha, Chun-HaoPaul Huang, TuanfengYang Wang, and  
547 Gordon Wetzstein. Generative rendering: Controllable 4d-guided video generation with 2d  
548 diffusion models. In *CVPR*, 2023a.
- 549 Shengqu Cai, EricRyan Chan, Songyou Peng, Mohamad Shahbazi, Anton Obukhov, LucVan Gool,  
550 and Gordon Wetzstein. Diffdreamer: Towards consistent unsupervised single-view scene extrap-  
551 olation with conditional diffusion models. In *ICCV*, 2023b.
- 552 Mathilde Caron, Hugo Touvron, Ishan Misra, Hervé Jégou, Julien Mairal, Piotr Bojanowski, and  
553 Armand Joulin. Emerging properties in self-supervised vision transformers. In *ICCV*, 2021.
- 554 Duygu Ceylan, Chun-HaoP Huang, and NiloyJ Mitra. Pix2video: Video editing using image diffusion.  
555 In *ICCV*, 2023.
- 556 Haoxin Chen, Menghan Xia, Yingqing He, Yong Zhang, Xiaodong Cun, Shaoshu Yang, Jinbo Xing,  
557 Yaofang Liu, Qifeng Chen, Xintao Wang, Chao Weng, and Ying Shan. Videocrafter1: Open  
558 diffusion models for high-quality video generation. *arXiv:2310.19512*, 2023.
- 559 Jadiel de Armas. Videoflow. <https://github.com/videoflow/videoflow>, 2019.
- 560 Yuwei Guo, Ceyuan Yang, Anyi Rao, Maneesh Agrawala, Dahua Lin, and Bo Dai. Sparsectrl: Adding  
561 sparse controls to text-to-video diffusion models. *arXiv:2311.16933*, 2023a.
- 562 Yuwei Guo, Ceyuan Yang, Anyi Rao, Yaohui Wang, Yu Qiao, Dahua Lin, and Bo Dai. Animatediff:  
563 Animate your personalized text-to-image diffusion models without specific tuning. In *ICLR*, 2023b.
- 564 Hao He, Yinghao Xu, Yuwei Guo, Gordon Wetzstein, Bo Dai, Hongsheng Li, and Ceyuan Yang.  
565 Cameractrl: Enabling camera control for text-to-video generation. *arXiv:2404.02101*, 2024.
- 566 Martin Heusel, Hubert Ramsauer, Thomas Unterthiner, Bernhard Nessler, and Sepp Hochreiter. Gans  
567 trained by a two time-scale update rule converge to a local nash equilibrium. In *NeurIPS*, 2017.
- 568 Alain Hore and Djemel Ziou. Image quality metrics: Psnr vs. ssim. In *ICPR*, 2010.
- 569 Li Hu, Xin Gao, Peng Zhang, Ke Sun, Bang Zhang, and Liefeng Bo. Animate anyone: Consistent and  
570 controllable image-to-video synthesis for character animation. *arXiv preprint arXiv:2311.17117*,  
571 2023.
- 572 HuEdward J., Yulong Shen, Phillip Wallis, Zeyuan Allen-Zhu, Yuanzhi Li, Shean Wang, and Weizhu  
573 Chen. Lora: Low-rank adaptation of large language models. In *ICLR*, 2022.
- 574 Levon Khachatryan, Andranik Movsisyan, Vahram Tadevosyan, Roberto Henschel, Zhangyang Wang,  
575 Shant Navasardyan, and Humphrey Shi. Text2video-zero: Text-to-image diffusion models are  
576 zero-shot video generators. In *ICCV*, 2023.
- 577 Diederik P. Kingma and Jimmy Ba. Adam: A method for stochastic optimization. In Yoshua Bengio  
578 and Yann LeCun (eds.), *3rd International Conference on Learning Representations, ICLR 2015,*  
579 *San Diego, CA, USA, May 7-9, 2015, Conference Track Proceedings*, 2015.
- 580 Yuheng Li, Haotian Liu, Qingyang Wu, Fangzhou Mu, Jianwei Yang, Jianfeng Gao, Chunyuan Li,  
581 and YongJae Lee. Gligen: Open-set grounded text-to-image generation. In *CVPR*, 2023.
- 582 Lu Ling, Yichen Sheng, Zhi Tu, Wentian Zhao, Cheng Xin, Kun Wan, Lantao Yu, Qianyu Guo, Zixun  
583 Yu, Yawen Lu, et al. D13dv-10k: A large-scale scene dataset for deep learning-based 3d vision. In  
584 *CVPR*, 2024.

- 594 Chong Mou, Xintao Wang, Liangbin Xie, Jian Zhang, Zhongang Qi, Ying Shan, and Xiaohu Qie.  
595 T2i-adapter: Learning adapters to dig out more controllable ability for text-to-image diffusion  
596 models. *arXiv:2302.08453*, 2023.
- 597 Haomiao Ni, Changhao Shi, Kai Li, Sharon X. Huang, and Martin Renqiang Min. Conditional  
598 image-to-video generation with latent flow diffusion models. In *2023 IEEE/CVF Conference*  
599 *on Computer Vision and Pattern Recognition (CVPR)*, pp. 18444–18455, 2023. doi: 10.1109/  
600 CVPR52729.2023.01769.
- 602 Hyeonwoo Noh, Seunghoon Hong, and Bohyung Han. Learning deconvolution network for semantic  
603 segmentation. In *Proceedings of the IEEE international conference on computer vision*, pp.  
604 1520–1528, 2015.
- 605 Elia Peruzzo, Vidit Goel, Deji Xu, Xingqian Xu, Yifan Jiang, Zhangyang Wang, Humphrey  
606 Shi, and Nicu Sebe. Vase: Object-centric appearance and shape manipulation of real videos.  
607 *arXiv:2401.02473*, 2024.
- 609 Robin Rombach, Andreas Blattmann, Dominik Lorenz, Patrick Esser, and Björn Ommer. High-  
610 resolution image synthesis with latent diffusion models. In *CVPR*, 2022.
- 611 Chitwan Saharia, William Chan, Saurabh Saxena, Lala Li, Jay Whang, Emily Denton, Seyed Kamyar,  
612 Seyed Ghasemipour, Burcu Karagol, SSara Mahdavi, RaphaGontijo Lopes, Tim Salimans, Jonathan  
613 Ho, DavidJ Fleet, and Mohammad Norouzi. Photorealistic text-to-image diffusion models with  
614 deep language understanding. In *NeurIPS*, 2022.
- 615 Johannes L. Schönberger and Jan-Michael Frahm. Structure-from-motion revisited. In *CVPR*, 2016.
- 617 Xiaoyu Shi, Zhaoyang Huang, Fu-Yun Wang, Weikang Bian, Dasong Li, Yi Zhang, Manyuan  
618 Zhang, Ka Chun Cheung, Simon See, Hongwei Qin, Jifeng Dai, and Hongsheng Li. Motion-i2v:  
619 Consistent and controllable image-to-video generation with explicit motion modeling. In *ACM*  
620 *SIGGRAPH 2024 Conference Papers*, SIGGRAPH '24, New York, NY, USA, 2024. Association  
621 for Computing Machinery. ISBN 9798400705250. doi: 10.1145/3641519.3657497. URL  
622 <https://doi.org/10.1145/3641519.3657497>.
- 623 Vincent Sitzmann, Semon Rezkikov, Bill Freeman, Josh Tenenbaum, and Frédo Durand. Light field  
624 networks: Neural scene representations with single-evaluation rendering. In *NeurIPS*, 2021.
- 625 Jiaming Song, Chenlin Meng, and Stefano Ermon. Denoising diffusion implicit models.  
626 *arXiv:2010.02502*, 2020.
- 628 Thomas Unterthiner, Sjoerdvan Steenkiste, Karol Kurach, Raphaël Marinier, Marcin Michalski,  
629 and Sylvain Gelly. Towards accurate generative models of video: A new metric & challenges.  
630 *arXiv:2303.14207*, 2018.
- 631 Vikram Voleti, Chun-Han Yao, Mark Boss, Adam Letts, David Pankratz, Dmitrii Tochilkin, Chris-  
632 tian Laforte, Robin Rombach, and Varun Jampani. SV3D: Novel multi-view synthesis and 3D  
633 generation from a single image using latent video diffusion. In *ECCV*, 2024.
- 635 Jianyuan Wang, Nikita Karaev, Christian Rupprecht, and David Novotny. Vggsfm: Visual geometry  
636 grounded deep structure from motion. In *CVPR*, 2024a.
- 637 Shuzhe Wang, Vincent Leroy, Yohann Cabon, Boris Chidlovskii, and Jerome Revaud. Dust3r:  
638 Geometric 3d vision made easy. In *CVPR*, 2024b.
- 640 Z. Wang, A.C. Bovik, H.R. Sheikh, and E.P. Simoncelli. Image quality assessment: From error  
641 visibility to structural similarity. *TIP*, 2004.
- 642 Zhouxia Wang, Ziyang Yuan, Xintao Wang, Yaowei Li, Tianshui Chen, Menghan Xia, Ping Luo,  
643 and Ying Shan. Motionctrl: A unified and flexible motion controller for video generation. In  
644 *SIGGRAPH*, 2024c.
- 646 JayZhangjie Wu, Yixiao Ge, Xintao Wang, Weixian Lei, Yuchao Gu, Wynne Hsu, Ying Shan,  
647 Xiaohu Qie, and MikeZheng Shou. Tune-a-video: One-shot tuning of image diffusion models for  
text-to-video generation. In *ICCV*, 2023.

- 648 Jinbo Xing, Menghan Xia, Yong Zhang, Haoxin Chen, Wangbo Yu, Hanyuan Liu, Xintao Wang,  
649 Tien-Tsin Wong, and Ying Shan. Dynamicrafter: Animating open-domain images with video  
650 diffusion priors. *arXiv:2310.12190*, 2023.
- 651  
652 Dejia Xu, Weili Nie, Chao Liu, Sifei Liu, Jan Kautz, Zhangyang Wang, and Arash Vahdat. Camco:  
653 Camera-controllable 3d-consistent image-to-video generation. *arXiv preprint arXiv:2406.02509*,  
654 2024.
- 655 Shiyuan Yang, Liang Hou, Haibin Huang, Chongyang Ma, Pengfei Wan, Di Zhang, Xiaodong Chen,  
656 and Jing Liao. Direct-a-video: Customized video generation with user-directed camera movement  
657 and object motion. In *ACM SIGGRAPH 2024 Conference Papers*, pp. 1–12. ACM, July 2024. doi:  
658 10.1145/3641519.3657481. URL <http://dx.doi.org/10.1145/3641519.3657481>.
- 659 Sihyun Yu, Kihyuk Sohn, Subin Kim, and Jinwoo Shin. Video probabilistic diffusion models in  
660 projected latent space. In *CVPR*, 2023.
- 661  
662 Lvmin Zhang and Maneesh Agrawala. Adding conditional control to text-to-image diffusion models.  
663 In *ICCV*, 2023.
- 664  
665 Lvmin Zhang, Anyi Rao, and Maneesh Agrawala. Adding conditional control to text-to-image  
666 diffusion models. In *ICCV*, 2023.
- 667 Richard Zhang, Phillip Isola, Alexei A. Efros, Eli Shechtman, and Oliver Wang. The unreasonable  
668 effectiveness of deep features as a perceptual metric. In *CVPR*, 2018.
- 669  
670 Wang Zhao, Shaohui Liu, Hengkai Guo, Wenping Wang, and Yong-Jin Liu. Particlesfm: Exploiting  
671 dense point trajectories for localizing moving cameras in the wild. In *ECCV*, 2022.
- 672 Tinghui Zhou, Richard Tucker, John Flynn, Graham Fyffe, and Noah Snavely. Stereo magnification:  
673 learning view synthesis using multiplane images. *TOG*, 2018.
- 674

## 675 A METRICS OF THE CAMERA TRAJECTORY CONTROLLABILITY

676  
677 Rotation Error: The relative rotation distances are then converted to radians, and we sum the total  
678 error of all frames,

$$680 R_{\text{err}} = \sum_{i=1}^n \arccos\left(\frac{\text{tr}(R_{\text{out}_i}^T R_{\text{gt}_i}^T) - 1}{2}\right) \quad (5)$$

681  
682 Translation Error: The norm of the relative translation vector for each frame is also summed together  
683 to form the translation error of the whole video,

$$684 T_{\text{err}} = \sum_{i=1}^n \|T_{\text{out}_i} - T_{\text{gt}_i}\|_2 \quad (6)$$

## 688 B ETHICS STATEMENT

689  
690 We strongly discourage the misuse of generative AI to create content that causes harm or spreads  
691 misinformation. Our camera trajectory-driven video generation approach could be abused to create  
692 misleading or invasive content, especially when fed malicious reference images. To mitigate these  
693 risks, we adhere to a strict code of ethics, respect privacy rights, comply with legal standards, and  
694 encourage positive adoption of our technology. We also recommend incorporating content safety  
695 mechanisms for the input image and generated video to prevent potential misuse, and we promote  
696 responsible use of the generated content.

697  
698  
699  
700  
701